

LESSONS FROM RANDOM MATRIX THEORY FOR QCD AT FINITE DENSITY

K. Splittorff

*The Niels Bohr Institute,
Blegdamsvej 17, Dk-2100, Copenhagen, Denmark
E-mail: split@nbi.dk*

J.J.M. Verbaarschot

*Stony Brook University,
Stony Brook, NY 11749-3800, USA
E-mail: jacobus.verbaarschot@stonybrook.edu*

In this lecture we discuss various aspects of QCD at nonzero chemical potential, including its phase diagram and the Dirac spectrum, and summarize what chiral random matrix theory has contributed to this subject. To illustrate the importance of the phase of the fermion determinant, we particularly highlight the differences between QCD and phase quenched QCD.

Keywords: QCD; Baryon Chemical Potential; Chiral Random Matrix Theory; Dirac Spectrum

1. Introduction

QCD at nonzero baryon chemical potential has turned out to be particularly challenging, and as of today, the phase diagram of QCD in the chemical potential temperature plane is far from being understood. There is not even agreement of its gross features such as the existence of a critical endpoint [1–3]. The reason for these difficulties is that the Dirac operator at nonzero chemical potential is nonhermitean resulting in a complex determinant so that the partition function cannot be evaluated by Monte-Carlo simulations. In this lecture we compare the QCD partition function to the QCD like partition function that only differs by the absence of the phase of the fermion determinant. This theory, known as phase quenched QCD, can be studied by means of lattice QCD simulations and has a phase diagram that is certainly completely different from QCD. This makes it clear that the phase of the fermion determinant is absolutely essential for the physics

of QCD at nonzero chemical potential.

In the second half of this lecture we will discuss various aspects of the phase of the fermion determinant and analyze its connections with the spectrum of the Dirac operator. We will do this in the context of chiral random matrix theory [4,5] at nonzero chemical potential [6–8]. In the microscopic domain [5], this theory is equivalent to QCD and, in spite of the fact that it can be solved analytically, it shares the sign problem and the physical effects of the phase of the fermion determinant with QCD.

2. Phase Diagram of QCD

The phase diagram of QCD in the temperature-chemical potential plane can only be obtained by means of nonperturbative methods. The method that has had the most impact is lattice QCD, but because it requires a real action, only the temperature axis has been studied extensively. The consensus is that, in the temperature range of 150-200 MeV, QCD undergoes a crossover transition from a chirally broken phase to a chirally symmetric phase. The picture at nonzero chemical potential is much less clear. Although significant progress has been made for small chemical potentials, questions about the structure of the phase diagram along the chemical potential axis could not be answered based on first principles (except for asymptotically large chemical potentials [9]). That is why most of our knowledge of QCD at nonzero baryon density is based on models and general properties of the phases of QCD.

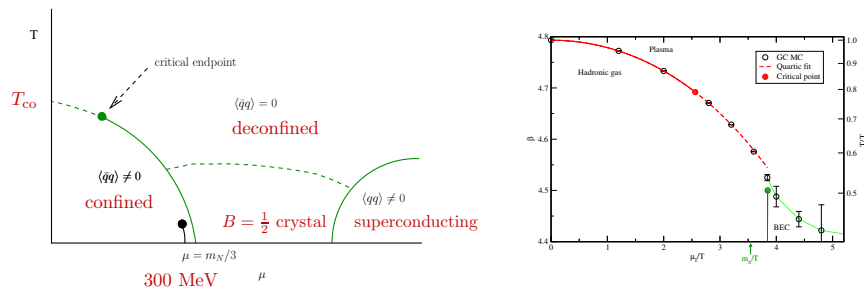


Fig. 1. The phase diagram of QCD in the temperature baryon chemical potential plane (left) and in the temperature isospin chemical potential plane (right). The data points in the right figure are from lattice QCD simulations [10].

A tentative phase diagram of QCD in the chemical potential temperature plane is shown in Fig. 1 (left). Among others we conjecture a chirally

symmetric crystalline phase made out of $B = \frac{1}{2}$ objects [11]. The best evidence for the existence of such phase is based on the Skyrme model where this phase exists as a strongly bound crystalline state with a binding energy of 135 MeV per nucleon (see Fig. 2 (left)). The chiral restoration phase transition to this phase is of second order for a face centered cubic crystal [12,13] but is of first order for a cubic crystal [14]. The restoration of chiral symmetry in the dense phase is illustrated by the vanishing of the average σ -field over a unit cell (see Fig. 2 (right)). When the temperature is increased, we expect that this crystal will melt at a temperature that is of the order of the binding energy. This phase has also been identified as the quarkyonic phase [15,16].

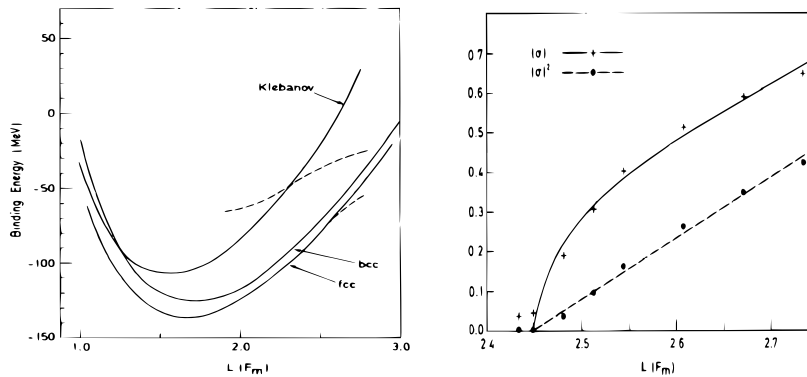


Fig. 2. Energy of a unit cell of a Skyrmion crystal (left) for a cubic crystal with cubic boundary conditions (obtained in [14]) and for a bcc and fcc crystal (obtained in [12]) versus the size of the unit cell. In the right figure we show the average value of the σ -field for an fcc crystal [12].

Our aim is to understand QCD at $\mu \neq 0$ from first principles, i.e. starting from the partition function

$$Z_{\text{QCD}} = \left\langle \prod_f \det(D + m_f + \mu\gamma_0) \right\rangle, \quad (1)$$

but the nonhermiticity of $D + \mu\gamma_0$ makes this a very challenging problem indeed. Let us first discuss the effect of the phase of the fermion determinant by studying the theory where this phase has been quenched. For $N_f = 2$ this partition function, known as phase quenched QCD, is given by

$$Z_{|\text{QCD}|} = \langle |\det(D + m + \mu\gamma_0)|^2 \rangle = \langle \det(D + m + \mu\gamma_0) \det(D + m - \mu\gamma_0) \rangle \quad (2)$$

Therefore, the chemical potential of phase quenched QCD can be interpreted as an isospin chemical potential [17], and at low enough temperatures, pions will Bose condense for $\mu > m_\pi/2$ [18–20]. This partition function can be simulated by Monte-Carlo methods [10,21–24] (see Fig. 1) and its phases are in agreement with theoretical expectations based on a mean field treatment of a chiral Lagrangian [18,25,26].

We conclude that for $\mu > m_\pi/2$ the phase factor quark determinant completely changes the phase diagram. The would be pion condensate is nullified by this phase factor after averaging. To better understand the effect of nonhermiticity, we will analyze the QCD partition function in the microscopic domain where it is equivalent to a chiral random matrix theory. This theory is analytically solvable in the nonperturbative domain of QCD, but the sign problem has all complications of QCD.

3. Random Matrix Model at $\mu \neq 0$

A chiral Random Matrix Theory (chRMT) is obtained by replacing the matrix elements of the Dirac operator by Gaussian random numbers [4,5]

$$D = \begin{pmatrix} 0 & iW^\dagger + \mu^\dagger \\ iW + \mu & 0 \end{pmatrix} \quad (3)$$

with W a complex $n \times (n+\nu)$ matrix, and μ is a multiple of the identity [6] or an arbitrary random matrix [8]. The random matrix partition function in the sector of topological charge ν is given by

$$Z_\nu(m_f; \mu) = \langle \prod_f \det(D + m_f) \rangle, \quad (4)$$

where the average is over the Gaussian distribution of W . This partition function has the global symmetries and transformation properties of QCD. At fixed θ -angle it is given by

$$Z(m_f, \theta; \mu) = \sum_\nu \mathcal{N}_\nu(\mu) e^{i\nu\theta} Z_\nu(m_f; \mu) \quad (5)$$

with $\mathcal{N}_\nu(\mu)$ s normalization constant that may depend on μ and ν .

In the microscopic domain of QCD, defined by

$$m_\pi^2 \ll \frac{1}{\sqrt{V}}, \quad \mu^2 \ll \frac{1}{\sqrt{V}}, \quad V\Lambda_{\text{QCD}}^4 \gg 1 \quad (6)$$

the mass and the chemical potential dependence of the QCD partition function is given by the random matrix partition function

$$Z_\nu^{\text{QCD}}(m; \mu) \sim Z_\nu^{\text{chRMT}}(m; \mu).$$

The reason for this equivalence is that in this domain, because the Compton wave length of the Goldstone modes is much larger than the size of the box, both theories reduce to the same static chiral Lagrangian. The Goldstone mass may either refer to physical quarks masses or to complex parameters (ghost quark masses) to probe the Dirac spectrum.

Since the kinetic term of the chiral Lagrangian does not contribute in a mean field analysis, chRMT correctly describes mean field results for the low-energy limit of QCD beyond the microscopic domain provided that $m \ll \Lambda_{\text{QCD}}$ and $\mu \ll \Lambda_{\text{QCD}}$.

4. Lessons from Random Matrix Theory

4.1. Lesson 1: Homogeneity of Dirac Eigenvalues

At nonzero chemical potential, the Dirac operator is nonhermitean with eigenvalues that are scattered in the complex plane. On inspection of quenched lattice QCD Dirac spectra (see Fig. 3) two properties stand out:

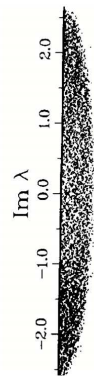


Fig. 3. Quenched Dirac eigenvalues on a $4^3 \times 8$ lattice [27].

i) The Dirac spectrum has a sharp edge, and ii) the distribution of the eigenvalues is more or less homogeneous. Both properties can be understood in terms of random matrix theory [6,7]. In essence they follow from the fact that eigenvalues of nonhermitean random matrices behave as repulsive electric charges in the plane. Because the chiral condensate is given by

$$\Sigma(m) = \frac{1}{V} \sum_{\lambda_k} \frac{1}{m + i\lambda_k},$$

it can be interpreted as the electric field at m of charges at λ_k . Therefore, a direct consequence of the homogeneity of the Dirac spectrum is that the quenched chiral condensate increases linearly with m when m is inside the domain of the eigenvalues.

4.2. Lesson 2: Quenched Limit

The quenched limit is the limit where the fermion determinant is ignored in generating the statistical ensemble. For zero chemical potential this has been a reasonable approximation, but at nonzero chemical potential, the limit of no fermion determinant is **not** given by

$$\lim_{n \rightarrow 0} \langle (\det(D + \mu\gamma_0 + m))^n \rangle,$$

but rather by

$$\lim_{m \rightarrow 0} \langle |\det(D + \mu\gamma_0 + m)|^n \rangle,$$

i.e. the quenched limit of phase quenched QCD [6]. Although similar ideas were proposed before [28,29], this result was first demonstrated convincingly for random matrix theory where the averages can be evaluated analytically.

Because phase quenched QCD is QCD at nonzero isospin chemical potential, a phase transition to a pion condensate occurs at $\mu = m_\pi/2$ for low temperatures. This phase is absent in full QCD where, at low temperatures a phase transition to a phase with nonzero baryon density occurs at $\mu = m_N/3$. We conclude that quenching completely fails for $\mu \neq 0$.

4.3. Lesson 3: Width of the Dirac Spectrum

The phase quenched partition function undergoes a phase transition at $\mu = m_\pi/2$. In terms of Dirac eigenvalues the only critical point occurs

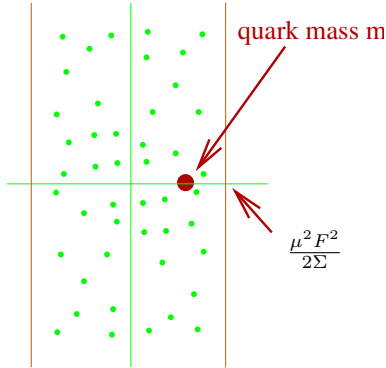


Fig. 4. Scatter plot of Dirac eigenvalues for quenched or phase quenched QCD at nonzero chemical potential.

when the quark mass hits the domain of eigenvalues (remember that it has a sharp edge). Therefore these two points have to coincide [28]. This leads to the following condition for the half-width m_c of the Dirac spectrum:

$$m_\pi^2 = \frac{2m_c \Sigma}{F^2} = 4\mu^2. \quad (7)$$

This result has also been derived from the static limit of the chiral Lagrangian for phase quenched QCD [19] which contains two low-energy constants, Σ and F_π , as parameters.

Since, at nonzero chemical potential

the low-lying Dirac spectrum is characterized by two quantities: the density of eigenvalues and the width of the spectrum, it is possible to extract Σ and F_π from these variables. More sophisticated methods to extract these constants from the low lying Dirac spectrum have been proposed and have been successfully applied to lattice QCD [30–38]. For sufficiently small chemical potential, when perturbation theory applies, the width of the Dirac spectrum increases linearly with μ rather than quadratically.

4.4. Lesson 4: Infrared Dominance

The question we wish to address in this section is whether the fluctuations of the fermion determinant given by

$$\det(D + m + \mu\gamma_0) = \prod_k (\lambda_k + m) \quad (8)$$

are dominated by the infrared part of the Dirac spectrum. At $\mu = 0$, because the low-energy limit of QCD is given by chiral perturbation theory for sufficiently small quark masses, this is apparently the case. This is less clear at $\mu \neq 0$ when the eigenvalues are complex. In particular, because the eigenvalue density for large λ increases as $\sim V\lambda^3$ one would expect that also the ultraviolet part of the Dirac spectrum contributes to the phase of the determinant. Although a nonzero chemical potential does not introduce new infinities once the theory is regularized at $\mu = 0$, one cannot exclude finite contributions from large Dirac eigenvalues.

When the chemical potential and the quark masses are in the microscopic domain of QCD, though, we can use random matrix theory to show that the average determinant is determined by the small Dirac eigenvalues. Further evidence for the infrared dominance of this quantity comes from lattice QCD at imaginary chemical potential, where a small number of low-lying eigenvalues reproduce the random matrix result [39].

Because of agreement with lattice QCD we know that chiral perturbation theory can be applied to phase quenched QCD when both the chemical potential and m_π are of order of F_π or less. This shows that the magnitude of the quark determinant is infrared dominated in this domain. Since the full QCD partition function in this domain does not depend on the chemical potential at low temperatures, in agreement with chiral perturbation theory, we conclude that the μ -dependence of the phase of the fermion determinant resides in the infrared part of the Dirac spectrum.

4.5. Lesson 5: Failure of Banks-Casher at $\mu \neq 0$

The Banks-Casher relation [40] states that

$$\Sigma = \lim_{m \rightarrow 0} \lim_{V \rightarrow \infty} \frac{\pi \rho(m)}{V}, \quad (9)$$

where $\rho(\lambda)$ is the density of Dirac eigenvalues and V is the volume of space-time. Although originally intended for a Hermitian Dirac operator, this relation correctly gives a vanishing chiral condensate for phase quenched QCD at $\mu \neq 0$. However, for full QCD at $\mu \neq 0$, the chiral condensate has

a discontinuity when the quark mass crosses the imaginary axis, but it does so without the occurrence of an accumulation of eigenvalues. The alternative mechanism that is at work has been understood in detail in random matrix theory [41,42]. For a comprehensive review we refer to the talk by Splittorff also in this volume [43]. Below we will illustrate this mechanism for QCD in one dimension which can also be viewed as a random matrix model.

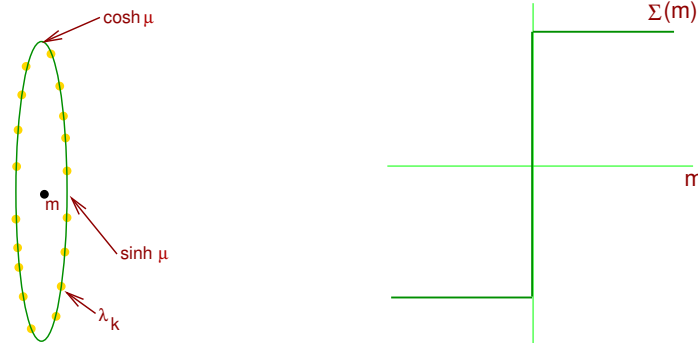


Fig. 5. Schematic plot of eigenvalues of the Dirac operator for lattice QCD in one dimension (left). The yellow dots denote the position of the eigenvalues for a single gauge field configuration, whereas the green ellipse shows the support of the spectrum in the thermodynamic limit. The chiral condensate for one flavor versus the quark mass is shown in the right figure.

The partition function of lattice QCD in one dimension is given by

$$Z = \int_{U \in U(N_c)} dU \det D, \quad (10)$$

where the integral is over the Haar-measure of $U(N_c)$. The Dirac operator is given by the $N \times N_c$ matrix (for N lattice points)

$$D = \begin{pmatrix} mI & e^\mu & \dots & e^{-\mu}U^\dagger \\ -e^{-\mu} & mI & \dots & 0 \\ \vdots & & & \vdots \\ 0 & \dots & mI & e^\mu \\ -e^\mu U/2 & \dots & -e^{-\mu} & mI \end{pmatrix}. \quad (11)$$

The chiral condensate for one flavor is defined by

$$\Sigma(m) = \frac{\left\langle \frac{1}{N} \sum_k \frac{1}{\lambda_k + m} \prod_k (\lambda_k + m) \right\rangle}{\left\langle \prod_k (\lambda_k + m) \right\rangle}. \quad (12)$$

Notice that the determinant has a complex phase. For $U(1)$ the chiral condensate can be evaluated analytically [44] with the result that is shown in

the right figure of Fig. 5. The amazing phenomenon, also known as the ‘‘Silver Blaze Problem’’ [45], is that the chiral condensate is continuous when m crosses the ellipse of eigenvalues, but shows a discontinuity at $m = 0$ where there are no eigenvalues. This can happen because the chiral condensate is determined by exponentially large (in the number of lattice points) contributions which cancel to give a finite result for the chiral condensate for $N \rightarrow \infty$.

4.6. Lesson 6: Quark Mass and Average Phase Factor

The severity of the sign problem can be measured through the expectation value of the average phase factor. A physical interpretation is obtained by defining the phase with respect to the phase quenched partition function:

$$\langle e^{2i\theta} \rangle_{\text{pq}} = \frac{\langle \det^2(D + m + \mu\gamma_0) \rangle}{\langle |\det(D + m + \mu\gamma_0)|^2 \rangle} \equiv \frac{Z_{\text{QCD}}}{Z_{|\text{QCD}|}}.$$

At nonzero temperature the free energies of QCD and $|\text{QCD}|$ are different so that the average phase factor vanishes in the thermodynamic limit.

At zero temperature, the free energy of QCD and phase quenched QCD are the same for $\mu < m_\pi/2$. Therefore, in the thermodynamic limit, the average phase factor is one for $\mu < m_\pi/2$. At finite volume, a nontrivial

μ -dependence is obtained from the one-loop corrections which give rise to an $O(1)$ contribution.

In the microscopic limit the average phase is given by the random matrix result that can be evaluated analytically (see Fig. 6 (right)). In the left part of the same figure we show a scatter plot of the Dirac eigenvalues of 40 200×200 random matrices. We conclude that, in the microscopic domain of QCD, the average phase factor vanishes if the quark mass is inside the support of the Dirac spectrum.

The average phase factor has been evaluated to one-loop order in chiral perturbation theory [46], and the results are in good agreement with lattice

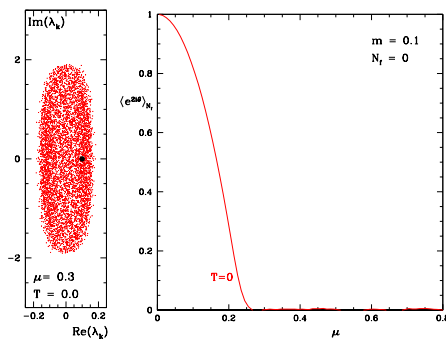


Fig. 6. Scatter plot of Dirac eigenvalues for chiral random matrix theory at nonzero chemical potential (left) and the average phase factor as a function of the chemical potential (right) for $m = 0.1$. In the left figure the mass is indicated by a black dot.

QCD [47]. The mean field limit of this result agrees with random matrix theory in the limit where the microscopic variables are large. Not surprisingly, also in the domain of chiral perturbation theory, the sign problem is most severe when the quark mass is inside the domain of eigenvalues.

4.7. Lesson 7: Distribution of Small Dirac Eigenvalues

One of the greatest successes of chiral random matrix theory has been the exact description of the distribution of the low-lying eigenvalues of the Dirac operator [4,5,48] both at zero (see review [49]) and at nonzero chemical potential (see review [50]). In this section we show recent results for the Dirac spectrum at nonzero chemical potential and topology. Such lattice calculations have become possible because of the introduction of an overlap Dirac operator at nonzero chemical potential [51]. In Fig. 7, the radial distribution of the lowest Dirac eigenvalue is shown for different values of the topological charge in comparison with analytical results derived in [52].

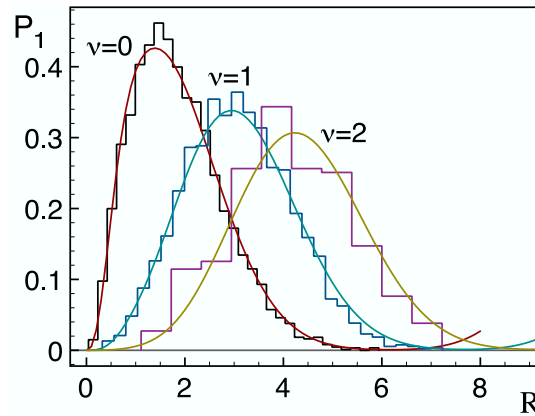


Fig. 7. Radial distribution of smallest Dirac eigenvalue for $\mu \neq 0$ in different topological charge sectors using a Dirac operator that satisfies the Ginsparg-Wilson relation (histograms) [52] compared to the prediction of chiral random matrix theory (smooth curve).

4.8. Lesson 8: Equality Two Condensates

The chiral condensate can be calculated in two ways

$$\Sigma^{(1)} = \lim_{m \rightarrow 0} \lim_{V \rightarrow \infty} \frac{1}{V} \left\langle \sum_k \frac{1}{\lambda_k + m} \right\rangle, \Sigma^{(2)} = \lim_{V \rightarrow \infty} \lim_{m \rightarrow 0} \frac{1}{V} \left\langle \sum_k \frac{1}{\lambda_k + m} \right\rangle, \quad (13)$$

where $\Sigma^{(1)}$ is nonzero because of spontaneous symmetry breaking, and its value does not depend on the total topological charge. The second chiral condensate can be expressed as

$$\Sigma^{(2)} = \lim_{V \rightarrow \infty} \frac{1}{V} \frac{\langle \prod_{\lambda_k \neq 0} \lambda_k \rangle_{\nu=1}}{\langle \prod_{\lambda_k} \lambda_k \rangle_{\nu=0}}. \quad (14)$$

The reason is that in the sector of topological charge ν , there are ν exact zero modes. The equality $\Sigma^{(1)} = \Sigma^{(2)}$ requires a subtle reshuffling of the eigenvalues: For $\nu = 1$ the eigenvalues are shifted by approximately half a level spacing w.r.t. $\nu = 0$ in order to satisfy the chiral Ward identity. Therefore, $\lambda_k^{\nu=1} \approx \sqrt{\lambda_k^{\nu=0} \lambda_{k+1}^{\nu=0}}$. To correctly normalize the ratio in (14) we evaluate it for a finite Dirac operator with an $N \times (N + \nu)$ nonzero off-diagonal block. Such Dirac matrix has ν exact zero eigenvalues (and perhaps additional paired zero modes which, being a set of measure zero, can be safely ignored). As it stands, the ratio (14) is dimensionally incorrect. A dimensionally correct ratio is obtained by replacing the largest squared eigenvalue pair for $\nu = 0$ by its square root, $[\lambda_N^{\nu=0}]^2 \rightarrow \lambda_N^{\nu=0}$. For the chiral condensate we then obtain the approximate expression

$$\Sigma^{(2)} = \frac{1}{V \lambda_{\min}}. \quad (15)$$

Using the Banks-Casher relation, the smallest nonzero eigenvalue is approximately given by

$$\lambda_{\min} \approx \frac{\pi}{2\Sigma V}, \quad (16)$$

resulting in $\Sigma^{(2)} \approx \frac{\pi}{2} \Sigma^{(1)}$. This calculation can be made rigorous (see [53]) with the result that both condensates become equal. Since we compare the ratio of two partition functions, it is essential that they are normalized correctly. This has been studied in a random matrix framework [53] confirming the above results.

Also within a random matrix framework, it turns out that for $\mu \neq 0$ the two condensate become only equal after the partition functions have been correctly normalized [54].

4.9. Lesson 9: Test of Algorithms

Because random matrix models are exactly solvable and show all essential features due to nonhermiticity, they are an ideal tool to test algorithms for lattice QCD at nonzero chemical potential. We mention two examples: i) The density of states method was analyzed and tested in a chiral ran-

dom matrix model at nonzero chemical potential [55] and has been applied successfully to lattice QCD [56,57]. ii) The radius of convergence has been determined [58] for algorithms that rely on Taylor expansion [47,59] or analytical continuation in μ [60,61].

5. Conclusions

We have shown that the phase of the fermion determinant dramatically affects the physics of the QCD partition function. For example, the phase diagram of QCD and $|\text{QCD}|$ are completely different. This is our main motivation for studying the behavior of the average phase factor and try to understand its relation with the spectrum of the Dirac operator. In particular, this has been done in the microscopic domain where QCD is given by a chiral random matrix theory that can be solved analytically. In this lecture we have discussed nine questions where random matrix theory has contributed significantly to our understanding of QCD at $\mu \neq 0$. Perhaps the most important contributions are the failure of the quenched approximation and the explanation of the mechanism that results in a discontinuity of the chiral condensate when the quark mass crosses the imaginary axis.

Acknowledgments: We wish to thank the organizer's of CAQCD 2008 for an inspiring week in Minneapolis as well as all of our colleagues who has contributed to the work reported here. This work was supported in part by U.S. DOE Grant No. DE-FAG-88ER40388. We thank the Institute for Nuclear Theory at the University of Washington for its hospitality and the Department of Energy for partial support during the completion of this work.

References

1. M. A. Stephanov, PoS **LAT2006**, 024 (2006) [arXiv:hep-lat/0701002].
2. Z. Fodor and S. D. Katz, JHEP **0404**, 050 (2004) [arXiv:hep-lat/0402006].
3. P. de Forcrand and O. Philipsen, arXiv:0808.1096 [hep-lat].
4. J. J. M. Verbaarschot, Phys. Rev. Lett. **72**, 2531 (1994) [arXiv:hep-th/9401059].
5. E. V. Shuryak and J. J. M. Verbaarschot, Nucl. Phys. A **560**, 306 (1993) [arXiv:hep-th/9212088].
6. M. A. Stephanov, Phys. Rev. Lett. **76**, 4472 (1996) [arXiv:hep-lat/9604003].
7. A. M. Halasz, J. C. Osborn and J. J. M. Verbaarschot, Phys. Rev. D **56**, 7059 (1997) [arXiv:hep-lat/9704007].
8. J. C. Osborn, Phys. Rev. Lett. **93**, 222001 (2004), [arXiv:hep-th/0403131].
9. D. T. Son, Phys. Rev. D **59**, 094019 (1999) [arXiv:hep-ph/9812287].
10. P. de Forcrand, M. A. Stephanov and U. Wenger, PoS **LAT2007**, 237 (2007) [arXiv:0711.0023 [hep-lat]].

11. A. S. Goldhaber and N. S. Manton, *Phys. Lett. B* **198**, 231 (1987).
12. L. Castillejo, P. S. J. Jones, A. D. Jackson, J. J. M. Verbaarschot and A. Jackson, *Nucl. Phys. A* **501**, 801 (1989).
13. A. D. Jackson and J. J. M. Verbaarschot, *Nucl. Phys. A* **484**, 419 (1988).
14. I. R. Klebanov, *Nucl. Phys. B* **262**, 133 (1985).
15. L. McLerran and R. D. Pisarski, *Nucl. Phys. A* **796**, 83 (2007) [arXiv:0706.2191 [hep-ph]].
16. Y. Hid aka, L. D. McLerran and R. D. Pisarski, *Nucl. Phys. A* **808**, 117 (2008) [arXiv:0803.0279 [hep-ph]].
17. M. G. Alford, A. Kapustin and F. Wilczek, *Phys. Rev. D* **59**, 054502 (1999) [arXiv:hep-lat/9807039].
18. J. B. Kogut, M. A. Stephanov, D. Toublan, J. J. M. Verbaarschot and A. Zhitnitsky, *Nucl. Phys. B* **582**, 477 (2000) [arXiv:hep-ph/0001171].
19. D. Toublan and J. J. M. Verbaarschot, *Int. J. Mod. Phys. B* **15**, 1404 (2001) [hep-th/0001110].
20. D. T. Son and M. A. Stephanov, *Phys. Rev. Lett.* **86**, 592 (2001) [arXiv:hep-ph/0005225].
21. S. Hands, I. Montvay, S. Morrison, M. Oevers, L. Scorzato and J. Skullerud, *Eur. Phys. J. C* **17**, 285 (2000) [arXiv:hep-lat/0006018].
22. J. B. Kogut and D. K. Sinclair, *Phys. Rev. D* **77**, 114503 (2008) [arXiv:0712.2625 [hep-lat]].
23. J. B. Kogut and D. K. Sinclair, *Phys. Rev. D* **77**, 114503 (2008) [arXiv:0712.2625 [hep-lat]].
24. J. B. Kogut and D. K. Sinclair, *Phys. Rev. D* **66**, 014508 (2002) [arXiv:hep-lat/0201017].
25. K. Splittorff, D. Toublan and J. J. M. Verbaarschot, *Nucl. Phys. B* **639**, 524 (2002) [arXiv:hep-ph/0204076].
26. G. V. Dunne and S. M. Nishigaki, *Nucl. Phys. B* **670**, 307 (2003) [arXiv:hep-ph/0306220].
27. I. Barbour, N. E. Behilil, E. Dagotto, F. Karsch, A. Moreo, M. Stone and H. W. Wyld, *Nucl. Phys. B* **275**, 296 (1986).
28. P. E. Gibbs, Glasgow preprint 86-0389 (unpublished).
29. A. Gocksch, *Phys. Rev. D* **37**, 1014 (1988).
30. M. E. Berbenni-Bitsch, A. D. Jackson, S. Meyer, A. Schafer, J. J. M. Verbaarschot and T. Wettig, *Nucl. Phys. Proc. Suppl.* **63**, 820 (1998) [arXiv:hep-lat/9709102].
31. J. C. Osborn and T. Wettig, *PoS LAT2005*, 200 (2006) [arXiv:hep-lat/0510115].
32. G. Akemann, J. C. Osborn, K. Splittorff and J. J. M. Verbaarschot, *Nucl. Phys. B* **712**, 287 (2005) [arXiv:hep-th/0411030].
33. G. Akemann, P. H. Damgaard, J. C. Osborn and K. Splittorff, *Nucl. Phys. B* **766**, 34 (2007) [Erratum-ibid. B **800**, 406 (2008)] [arXiv:hep-th/0609059].
34. G. Akemann and P. H. Damgaard, *JHEP* **0803**, 073 (2008) [arXiv:0803.1171 [hep-th]].
35. G. Akemann and P. H. Damgaard, *JHEP* **0803**, 073 (2008) [arXiv:0803.1171 [hep-th]].

36. P. H. Damgaard, U. M. Heller, K. Splittorff, B. Svetitsky and D. Toublan, Phys. Rev. D **73**, 105016 (2006) [arXiv:hep-th/0604054].
37. P. H. Damgaard, U. M. Heller, K. Splittorff, B. Svetitsky and D. Toublan, Phys. Rev. D **73**, 074023 (2006) [arXiv:hep-lat/0602030].
38. P. H. Damgaard, U. M. Heller, K. Splittorff and B. Svetitsky, Phys. Rev. D **72**, 091501 (2005) [arXiv:hep-lat/0508029].
39. K. Splittorff and B. Svetitsky, Phys. Rev. D **75**, 114504 (2007) [arXiv:hep-lat/0703004].
40. T. Banks and A. Casher, Nucl. Phys. **B169**, 103 (1980).
41. J. C. Osborn, K. Splittorff and J. J. M. Verbaarschot, Phys. Rev. Lett. **94**, 202001 (2005), [arXiv:hep-th/0501210].
42. J. C. Osborn, K. Splittorff and J. J. M. Verbaarschot, arXiv:0805.1303 [hep-th].
43. J. C. Osborn, K. Splittorff and J. J. M. Verbaarschot, this volume, arXiv:0808.1982 [hep-lat].
44. L. Ravagli and J. J. M. Verbaarschot, Phys. Rev. D **76**, 054506 (2007) [arXiv:0704.1111 [hep-th]].
45. T. D. Cohen, Phys. Rev. Lett. **91**, 222001 (2003) [arXiv:hep-ph/0307089].
46. K. Splittorff and J. J. M. Verbaarschot, Phys. Rev. D **77**, 014514 (2008) [arXiv:0709.2218 [hep-lat]].
47. C. R. Allton *et al.*, Phys. Rev. D **66**, 074507 (2002) [arXiv:hep-lat/0204010].
48. J.J.M. Verbaarschot and I. Zahed, Phys. Rev. Lett. **70**, 3852 (1993) [arXiv:hep-th/9303012].
49. J. J. M. Verbaarschot and T. Wettig, Ann. Rev. Nucl. Part. Sci. **50**, 343 (2000) [arXiv:hep-ph/0003017].
50. G. Akemann, Int. J. Mod. Phys. A **22**, 1077 (2007) [arXiv:hep-th/0701175].
51. J. Bloch and T. Wettig, Phys. Rev. Lett. **97**, 012003 (2006) [arXiv:hep-lat/0604020].
52. G. Akemann, J. Bloch, L. Shifrin and T. Wettig, Phys. Rev. Lett. **100**, 032002 (2008) [arXiv:0710.2865 [hep-lat]].
53. L. Shifrin and J. J. M. Verbaarschot, Phys. Rev. D **73**, 07400 [arXiv:hep-th/0507220].
54. C. Lehner, M. Otani, J.J.M. Verbaarschot and T. Wettig, in progress.
55. J. Ambjorn, K. N. Anagnostopoulos, J. Nishimura and J. J. M. Verbaarschot, JHEP **0210**, 062 (2002) [arXiv:hep-lat/0208025].
56. Z. Fodor, S. D. Katz and C. Schmidt, JHEP **0703**, 121 (2007) [arXiv:hep-lat/0701022].
57. S. Ejiri, arXiv:0804.3227 [hep-lat].
58. M. A. Stephanov, Phys. Rev. D **73**, 094508 (2006) [arXiv:hep-lat/0603014].
59. R. V. Gavai, S. Gupta and P. Majumdar, Phys. Rev. D **65**, 054506 (2002) [arXiv:hep-lat/0110032].
60. M. D'Elia and M. P. Lombardo, Phys. Rev. D **67**, 014505 (2003) [arXiv:hep-lat/0209146].
61. P. de Forcrand and O. Philipsen, Nucl. Phys. B **642**, 290 (2002) [arXiv:hep-lat/0205016].